Novel antibodies targeting the N-terminus of FGF19 inhibit hepatocellular carcinoma growth without bile-acid-related side effects

Huisi Liu, Sanduo Zheng, Xinfeng Hou, Ximing Liu, Kaxin Du, Xueyuan Lv, Yulu Li, Fang Yang, Wenhui Li, Jianhua Sui*

This file includes supporting information:

1. Supporting figures 1-6.

2. Supporting tables 1-2.

Fig. S1

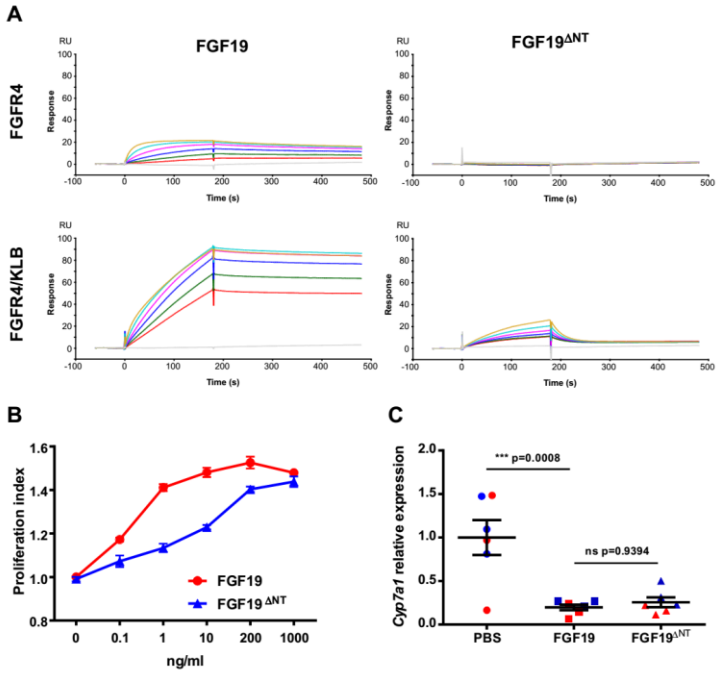

Figure S1. Dispensable role of the FGF19's N-terminus in mediating FGF19's *Cyp7a1*-regulating activity. (A) The N-terminus deletion variant FGF19$^{\Delta NT}$ has reduced binding affinity for FGFR4. Kinetic analyses of FGF19 or FGF19$^{\Delta NT}$ binding to FGFR4 were performed on a Biacore T200 (GE Healthcare Life Sciences) at 25ºC. Anti-human IgG Fc antibody was covalently attached to individual flow cell surfaces of a CM5 sensor chip by amine-coupling using the amine coupling kit (GE Healthcare Life Sciences). FGFR4-hFc was captured as a ligand on the CM5 chip. Interactions between ligand FGFR4 and analytes FGF19 or FGF19$^{\Delta NT}$ were measured in the presence of 20 μg/ml heparin and with (top panel) or without co-receptor β-klotho (bottom panel). Analytes were in 2-fold serial dilution starting from 1000 nM. **(B)** N-terminus deletion variant FGF19$^{\Delta NT}$ showed reduced activity to induce cell proliferation. Hep3B cells were cultured with different concentrations of FGF19 or FGF19$^{\Delta NT}$ in 1% FBS containing DMEM. **(C)** N-terminus deletion variant FGF19$^{\Delta NT}$ retained the ability to suppress *Cyp7a1* gene expression *in vivo*. C57BL/6 mice were fasted before intraperitoneal injection with the indicated treatments. Hepatic gene expression of *Cyp7a1* was analyzed by qPCR. Each treatment group consisted of 3 male (blue) and 3 female (red) mice.

Fig. S2

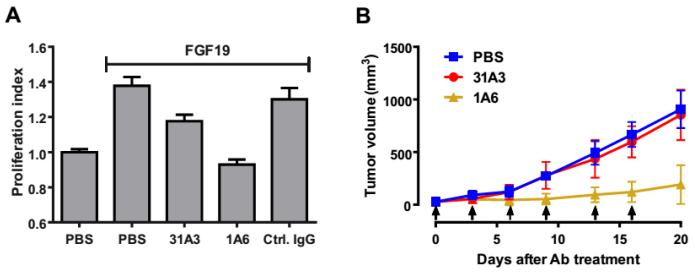

Figure S2. Characterization of the 31A3 antibody. (A) 31A3 inhibits FGF19-induced cell proliferation. Hep3B cells were cultured with 20 ng/ml FGF19 and 100 nM antibodies in 1% FBS containing DMEM. Control IgG, Rituximab. **(B)** 31A3 cannot suppress tumor growth in a xenograft mouse model. Hep3B (s.c.) tumor-bearing NSG mice were divided into groups (n=4/group) with equivalent mean tumor volume and received treatment of 31A3, 1A6, or PBS. Tumor growth was measured by caliper. Antibody treatment is marked by arrows.

Fig. S3

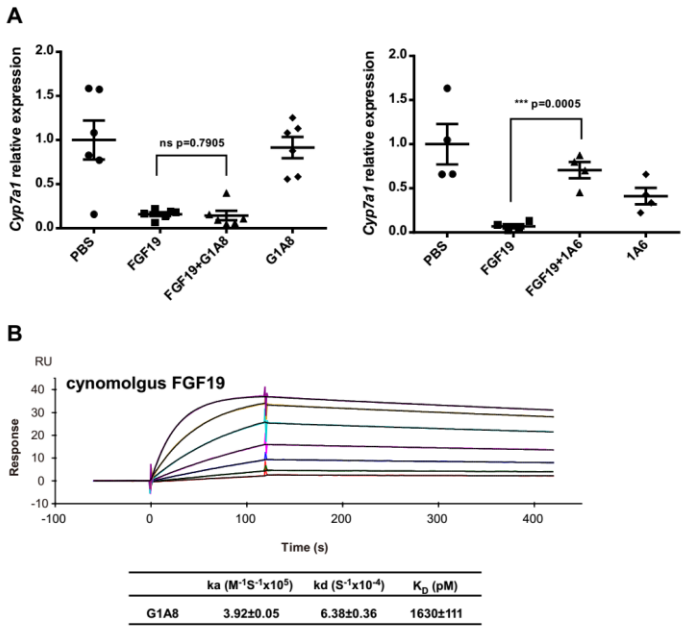

	ka ($M^{-1}S^{-1}x10^5$)	kd ($S^{-1}x10^{-4}$)	K_D (pM)
G1A8	3.92±0.05	6.38±0.36	1630±111

Figure S3. Safety evaluation of G1A8. (A) G1A8 does not impair mouse hepatic *Cyp7a1* gene expression down-regulated by FGF19. C57BL/6 mice were fasted before intraperitoneal injection with the indicated treatments. The hepatic *Cyp7a1* gene expression level was analyzed by qPCR. G1A8 and 1A6 were in 5-fold molar ratio of FGF19. **(B)** Kinetic analysis of the binding of G1A8 to the cynomolgus FGF19 (two-fold serial dilutions from 100 nM) using SPR (Biacore T200).

Fig. S4

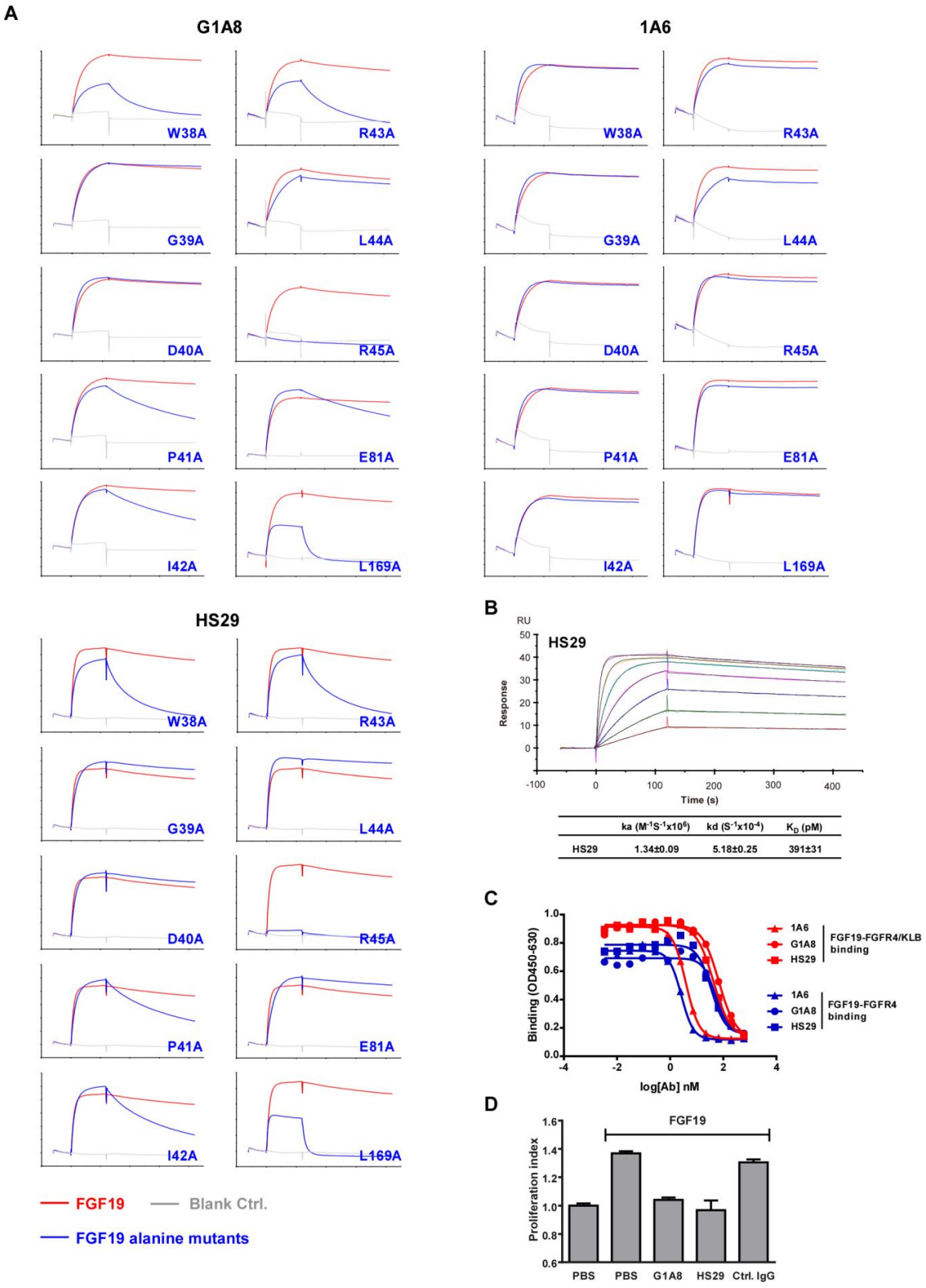
A
G1A8
1A6
HS29
W38A
R43A
G39A
L44A
D40A
R45A
P41A
E81A
I42A
L169A
FGF19
Blank Ctrl.
FGF19 alanine mutants
B
HS29
RU
Response
Time (s)
ka (M-1S-1x10^5) kd (S-1x10-4) KD (pM)
HS29 1.34±0.09 5.18±0.25 391±31
C
Binding (OD450-630)
log[Ab] nM
1A6
G1A8
HS29
FGF19-FGFR4/KLB binding
FGF19-FGFR4 binding
D
FGF19
Proliferation index
PBS
PBS
G1A8
HS29
Ctrl. IgG

Figure S4. Epitope mapping and *in vitro* characterization of anti-FGF19 antibodies. (A) Binding analysis between anti-FGF19 antibodies (G1A8, HS29 and 1A6) to FGF19 alanine mutants analyzed using SPR (Biacore T200). FGF19 alanine mutants were tested at 50 nM. Single alanine substitution introduced at these tested residues does not affect the overall folding structure of FGF19; all FGF19 alanine mutants tested had very similar binding affinities to the reference antibody 1A6, which is known to target amino acids 136-158 of the C-terminal region of FGF19 (*15*). **(B)** Kinetic analysis of the binding of HS29 to FGF19. FGF19 was in two-fold serial dilutions from 100 nM. **(C)** Competition activity of anti-FGF19 antibodies (G1A8, HS29 and 1A6) against FGF19 for binding to FGFR4. An ELISA-based competition binding assay was used. FGF19 protein was first captured on an ELISA plate; antibodies in their Fab form were mixed with 100 nM FGFR4-hFc in the presence of 20 μg/ml heparin with or without 0.5μg/ml co-receptor KLB, and then added to the ELISA plate. The binding of FGFR4-hFc to FGF19 was detected by using HRP-anti-hFc secondary antibody. **(D)** HS29 inhibits FGF19-induced cell proliferation. Hep3B was cultured with 20 ng/ml FGF19 and 100 nM antibodies. Control IgG, Rituximab.

Fig. S5

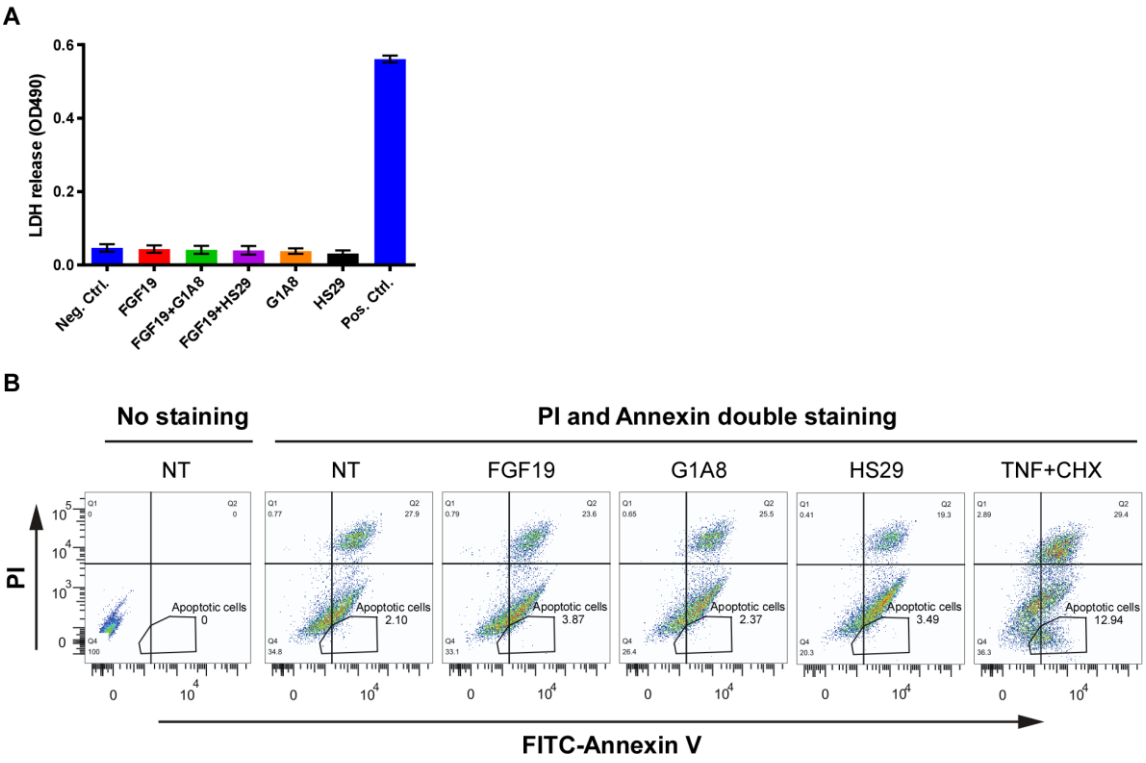

Fig S5. Assessment of the cytotoxic and apoptotic effects of G1A8 and HS29. (A) Analysis of the cytotoxicity effect of G1A8 and HS29 using a LDH release assay. The Hep3B cells ($1x10^4$/well, in DMEM supplemented with 1% FBS) were treated with testing antibodies (15 μg/ml) in the presence or absence of FGF19 (20ng/ml) for 48 hrs. Each treatment was performed in triplicate. The cytotoxicity was assessed by measuring LDH release level in the culture supernatants using CytoTox 96® Non-Radioactive Cytotoxicity Assay kit (Promega). No treatment cells served as the negative control; no treatment cells lysed with the kit's lysis buffer at the end of the experiment served as the positive control. **(B)** Analysis of the apoptotic effect of G1A8 and HS29 using Propidium Iodide (PI)/Annexin V double staining. The Hep3B cells were treated with antibodies (15ug/ml) or FGF19 (20ng/ml) for 72 hrs; or treated with TNFα (20ng/ml) and cycloheximide (CHX, 10ug/ml) for 6 hrs (served as a positive control for induction of apoptosis). At the end of the experiment, the cells were harvested for staining with FITC-conjugated Annexin V and PI, and were analyzed by flow cytometry.

Fig. S6

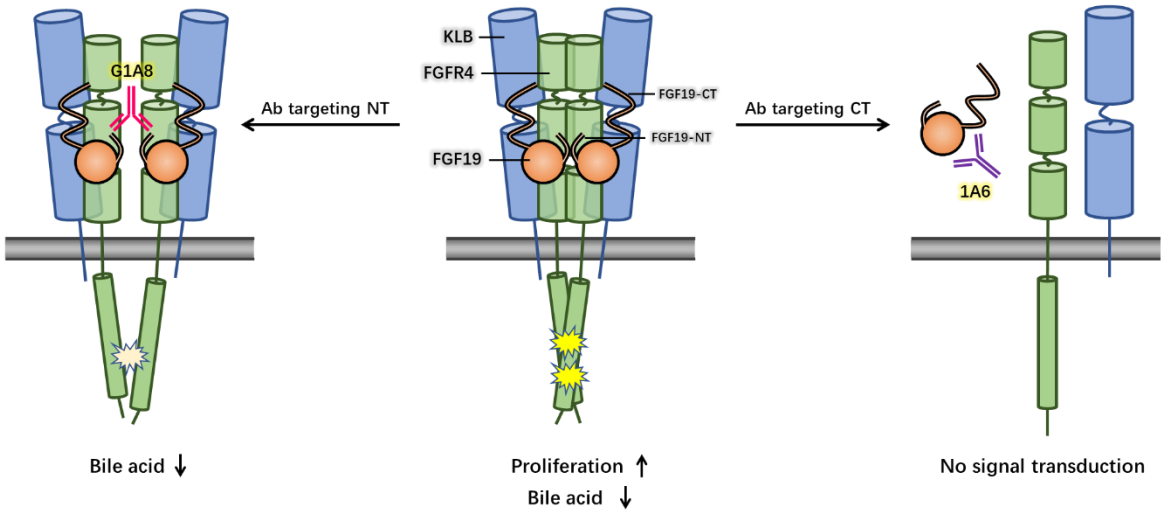

Fig S6. Schematic diagrams of proposed mechanism-of-action of anti-FGF19 antibodies. A hypothetical model of a dimeric FGF19–KLB-FGFR4 ternary receptor complex and signaling is shown in the middle panel. 1A6 antibody targeting an epitope proximal to the CT blocks FGF19 binding to KLB, and thus blocking receptor tethering and the formation a stable ternary receptor complex, as well as the subsequent receptor complex dimerization. As a result, 1A6 antibody treatment leads to a complete loss of FGF19's activities, including its physiological activity (*Right*). G1A8 antibody targeting FGF19's globular NT may not affect the formation of ternary receptor complex, but interfere with receptor dimerization or other mechanism(s), thus reducing receptor signaling strength. As a result, G1A8 antibody treatment maintains FGF19's bile-acid-regulatory function (*Left*).

Table S1. Crystallographic statistics

	FGF19-G1A8
Data collection*	
Wavelength (Å)	0.9789
Space group	$P2_12_12_1$
Unit cell dimensions	
a, b, c (Å)	85.0, 104.1, 165.4
α, β, γ (°)	90.0, 90.0, 90.0
Resolution (Å)	48.73 – 2.6 (2.69 – 2.60)
Completeness (%)	99.7 (99.0)
<I/σ(I)>	24.3 (3.3)
$CC_{1/2}$ (%)	99.7 (95.2)
R_{merge} (%)	1.7(14.5)
Multiplicity	2.0 (2.0)
Refinement	
Resolution (Å)	48.7 – 2.6 (2.66 – 2.60)
No. reflections	45834 (3207)
R_{work}/R_{free} (%)	20.0 / 25.2 (35.1/40.1)
No. atoms	8740
B factors (Å^2)	63.9
RMS deviation	
Bond length (Å)	0.005
Bond angles (°)	0.833
Ramachandran statistics	
Favored	96.37%
Allowed	3.63%
Outliers	0

*Values in parentheses are for highest shell.

Table S2. Contact residues between G1A8 and FGF19

G1A8	HCDR1	HCDR2		HCDR3					LCDR1	LCDR2			LCDR3	
	A33	S52	S57	N100	W101	Q102	E103	L104	Y34	Y51	D52	P57	W93	R95
FGF19	W38	W38	W38	R45	I42, L44, E81	W38, I42	R45	W38	P41, R43	R45, P167, L169	R45	L169	P41	D40

Contact residues with interatomic distances less than 4 Å are summarized. Residues involved in hydrogen bond or salt bridge interactions are colored in red.